Simulation Standard

TCAD Driven CAD

A Journal for Process and Device Engineers

A Model for Boron T.E.D. in Silicon: Full Couplings of Dopant with Free and Clustered Interstitials

F. Boucard1,2,3, D. Mathiot1, E. Guichard2, and P. Rivallin3
1 Laboratoire PHASE-CNRS, 23 rue du Loess, F-67037 Strasbourg Cedex 2, France
2 SILVACO DATA SYSTEMS , 55, rue Blaise Pascal, F-38330 Montbonnot, France
3 LETI-CEA, 17 Av. des Martyrs F-38054 Grenoble cedex 9, France

Abstract

In this contribution we present a model for transient enhanced diffusion of boron in silicon. This model is based on the usual pair diffusion mechanism including non-equilibrium reactions between the dopant and the free point defects, taking into account their various charge states. In addition to, and fully coupled with the dopant diffusion we model the growth and dissolution of the interstitials and boron interstitials clusters associated with the anneal of the self-interstitial supersaturation created by the implantation step. It is thus possible to simulate a rather large set of experimental conditions, from conventional predeposition steps, to RTA after low energy implantation.

Introduction

One of the most important challenges in developing ULSI technology today is to shrink device sizes to their limit. Each generation requires a large effort in research and development, where technological computer aided design (TCAD) can play a key role.

Ion implantation is the common technique used for doping advanced silicon devices in microelectronics. However this technique induces a huge supersaturation of point defects in the Si crystal which leads to an anomalous broadening of the dopant profile during the high temperature activation anneal. This phenomenon, known as transient enhanced diffusion (TED) is particularly noticeable and embarrassing for boron diffusion, where it is a serious issue for the formation of the ultra shallow junctions needed for next generation of devices. It is also now well established that TED is strongly correlated with the evolution of the self-interstitial supersaturation governed by the nucleation and evolution, during the high temperature anneal, of a variety of extended defects structures like boron interstitial clusters (BIC) [1] or interstitials clusters (IC) [2].

Thus, predictive process modeling, needed for deep submicron MOSFET technologies, requires the development of accurate diffusion models taking into account the full set of interactions between the dopant and the point or extended defects (clusters). The purpose of this contribution is to show that it is possible to extend the usual dopant pair diffusion model to take into account these interstitial-related clusters. Special attention is paid on the fact that the "new" model is fully consistent with the equilibrium "normal" model.

Basic Diffusion Mechanism

As a starting point of our modeling effort we used an extension of the basic dopant pair diffusion model proposed several years ago by one of us [3]. Briefly, the basic idea of this model is that isolated substitutional boron atoms (BS) are immobile. The dopant diffusion occurs only via the diffusion of boron / self-interstitial (BI) and (to a less extend) of boron / vacancy (BV) pairs. However, in the present work, we do not assume local equilibrium between the pairs and their components. As previously, we considered all the possible charge states of the free defects and of the pairs, the rel-

Continued on page 2....

INSIDE

SILVACO INTERNATIONAL

ative concentrations of which depend on the local Fermi level position. Since we want to be able to handle experimental cases where, as after ion implantation, the defect concentrations are of the same order of magnitude or even higher than the dopant concentration, the concentrations of all the charged species (dopant, free point defects, pairs and clusters) are accounted for in the neutrality equation used to compute the electron concentration. Nevertheless, since electronic exchanges are extremely faster than atomic reactions, we assume that the various charge states of a given species are always in local equilibrium, and thus, in order to minimize the number of equations, we explicitly describe only one reaction path for the formation of each pair, the other charge states being consistently computed through the position of the defect related deep level. The pairing reactions between the dopant and point-defects explicitly considered in the present work are the following :

$$B_S^- + I^0 \underset{k_s^r}{\overset{k_s^f}{\rightleftharpoons}} BI^-$$

$$B_S^- + V^+ \underset{k_s^r}{\overset{k_s^f}{\rightleftharpoons}} BV^0$$

$$BI^- + V^0 \underset{k_c^r}{\overset{k_c^f}{\rightleftharpoons}} B_S^-$$

$$BV^0 + I^0 \underset{k_d^r}{\overset{k_d^f}{\rightleftharpoons}} B_S^- + h^+$$

The evolution of the boron and free defect concentrations are then given by the following set of continuity equations :

$$\frac{\partial [B_S]}{\partial t} = -\frac{\partial J_B^{tot}}{\partial x} - \Sigma \left(\frac{\partial [BI^i]}{\partial t} + \frac{\partial [BV^i]}{\partial t} \right) + (G - R)_{BIC}$$

$$\frac{\partial [I]}{\partial t} = -\frac{\partial J_I}{\partial x} - \Sigma \left(\frac{\partial [BI^i]}{\partial t} \right) - R_{I/V} + (G - R)_{In} + (G - R)_{BIC}$$

$$\frac{\partial [V]}{\partial t} = -\frac{\partial J_V}{\partial x} - \Sigma \left(\frac{\partial [BV^i]}{\partial t} \right) - R_{I/V}$$

where the various fluxes (JX) include built-in field drift effects on charged species and RI/V account for the bimolecular recombination between self-interstitials (I) and vacancies (V) [3]. The additional (G-R)In and (G-R)BIC terms account for the generation or consumption of the various species due to the interstitial-related clusters formation and dissolution as described in the following sections.

From these continuity equations solved by PROMIS [5], boron profiles can be theoretically calculated in any experimental situation if appropriate initial conditions are assumed for the point defects. As a first indication of the ability of our model to handle the complex couplings between boron and the free point defects, we show on Figure1 the results of the simulation of conventional predeposition steps (diffusion with a constant surface concentration), where the initial concentrations of the defects are assumed to have their equilibrium values. For this specific case the (G-R) terms linked to the interstitial-related clusters evolution vanish, and such simulations can thus be used to fit the basic parameters describing the dopant interactions with the free point

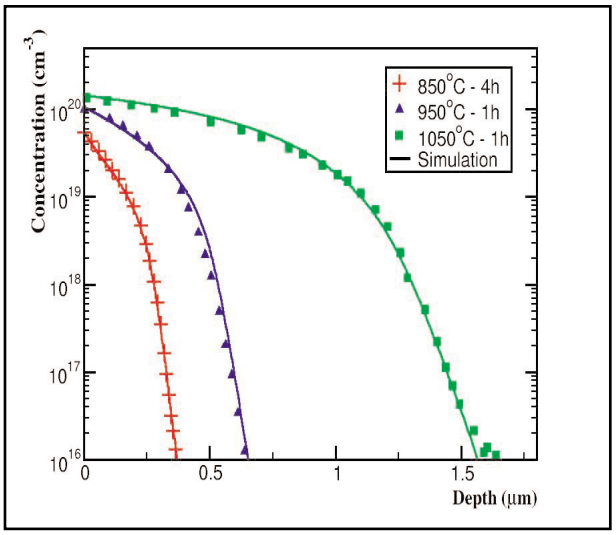

Figure 1. Comparison between calculated and experimental boron predeposition profiles. Experimental data are from ref. [4]

defects. As shown on Figure 1, the agreement between the experimental profiles [4] and the simulated ones, with parameters corresponding to a I contribution to the total B diffusion of the order of 85 %, is remarkably good.

Interstitial Clusters

In order to be able to simulate the T.E.D. of boron, the basic pair diffusion model is fully coupled, through generation and recombination terms, to the equations describing the evolution of the point defects in connection with the growth and dissolution of interstitial clusters.

For this purpose we describe the kinetics of the IC's using the model we developed recently for the growth of {311} defects [6]. In this model, a cluster containing n interstitials evolve to a cluster of size n+1 by interaction with a free interstitial in agreement to the following reactions with the corresponding relations describing the time evolution of the various concentrations :

$$I^{free} + I^{free} \underset{k_2^r}{\overset{k_2^f}{\rightleftharpoons}} I_2$$

$$I_2 + I^{free} \underset{k_3^r}{\overset{k_3^f}{\rightleftharpoons}} I_3 \quad \Leftrightarrow \quad \begin{cases} \frac{\partial [I^{free}]}{\partial t} = 2(k\,[I^{free}]^2 - k_2^r [I_2]) + \sum_{j=3}^{Nmax} k\,[I^{free}][I_{j-1}] - k_j^r [I_j] \\ \frac{\partial [I_2]}{\partial t} = k_2^f [I^{free}]^2 - k_2^r [I_2]) - k_3^f [I^{free}]\,[I_2] + k_3^r [I_3] \\ \frac{\partial [I_j]}{\partial t} = k_j^f [I^{free}]\,[I_{j-1}] - k_j^r [I_j] - k_{j-1}^f [I^{free}][I_j] = k_{j-1}^r [I_{j-1}] \end{cases}$$

$$I_{n-1} + I^{free} \underset{k_n^r}{\overset{k_n^f}{\rightleftharpoons}} I_n$$

According to [6], the various rate constants are given by

$$\begin{cases} k_n^f = 4\pi\, r_n^{eff} D_I . \exp\left(\frac{\Delta g_n}{kT} \right) \\ \Delta g_n = \max\left(-kT \ln\left(\frac{[I^{free}]}{[I]^{eq}} \right) + E_f(n); 0 \right) \\ k_n^r = 6 \frac{D_I}{\lambda^{2-n}} \theta \,.\exp\left(\frac{E_f^I(n) - E_f^I}{kT} \right) \end{cases}$$

where r_n^{eff} is the effective capture radius of the defect of size n, Δg_n is the effective energy barrier that an interstitial must overcome, $E_f(n)$ is the energetic cost for

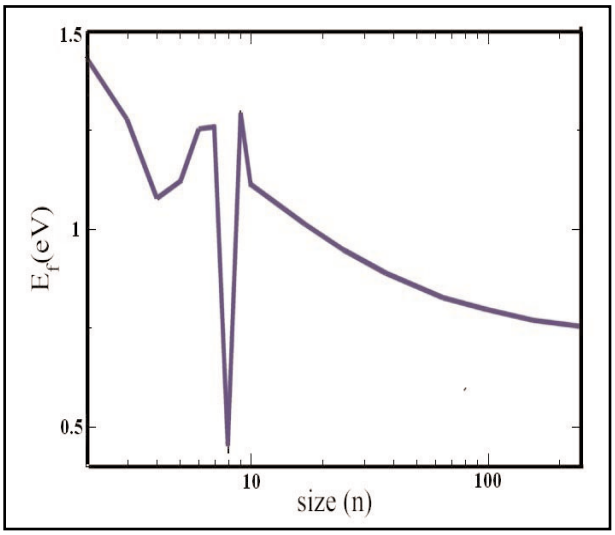

Figure 2. Fitted formation energy per atom included in a cluster of size n

adding one Si atom to a cluster of size n, i.e. the formation energy per I atom in the cluster of size n, E_f^I is the formation energy for an isolated self-interstitial, θ_n is the number of dissociation sites, and λ is the lattice distance [6].

The validity of the interstitial cluster growth model is tested by comparing its predictions with the experimental data obtained by Cowern et al. [7]. Briefly, this experiment consists in measuring the enhanced diffusivity of two buried boron marker layers induced by a superficial silicon implantation at 40 keV with a dose of 2.10^{13} at/cm^2. To start the calculation, we used here a simple +1 model to describe the initial self-interstitial concentration induced by the Si implant. In order to obtain the best fit, the values of the various formation energies have to be slightly changed as compared to the initial values proposed by Cowern et al. We think that this is due to the fact that the way we estimate the formation rate constant k_n is somewhat different. In our model, this rate constant depends on the current free self-interstitial supersaturation, in such a way that the formation can be reaction limited for small sizes when the I supersaturation has significantly decreased [6]. However, in agreement with Cowern et al., we found that good fits is possible only by considering some stable "magic" sizes, i.e. cluster containing 4 and 8 atoms. For clusters of size larger than 10 we used {311} formation energies tending asymptotically toward 0.67 eV for large values of n, as depicted on Figure 2.

The corresponding calculated curves are given on Figure 3. On Figure 3(a) we show the excellent agreement between the calculated evolution of the self-interstitial supersaturation as compared to the values extracted from the experimental profile broadening. It is emphasized that our approach allows a particularly nice description of the time evolution of the I supersaturation, especially for low thermal budgets. Since our I evolution model is coupled with the B diffusion equations, it is then possible to simulate the corresponding B broadening. The calculated B profiles are shown on Figure 3(b), and exhibit all the features experimentally observed in [7], i.e. the exponential low concentration tail for low thermal budgets evolving to symmetrically broadened profiles for longer times.

Boron Interstitial Cluster Formation

The simulation of Cowern and coworker's experiment presented above is possible without taking into account the boron interstitial complexes formation, because the boron concentration is low enough. However, when a high concentration of free self-interstitials co-exists with a significant boron concentration, even below the solubility limit, as for example when crystalline silicon is implanted with medium doses of boron, the presence of these

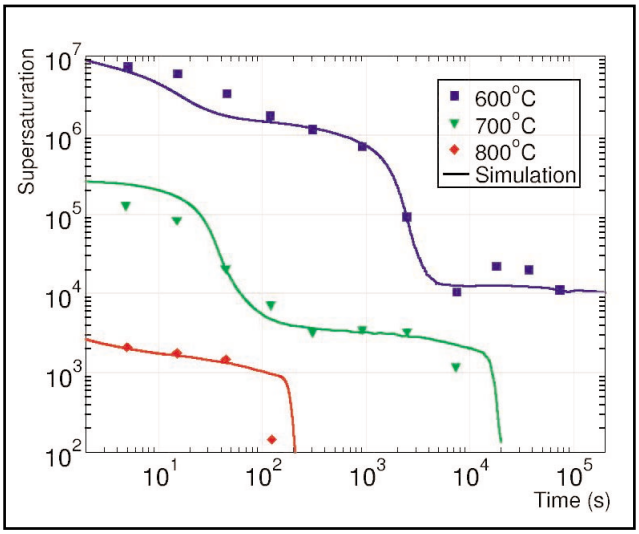

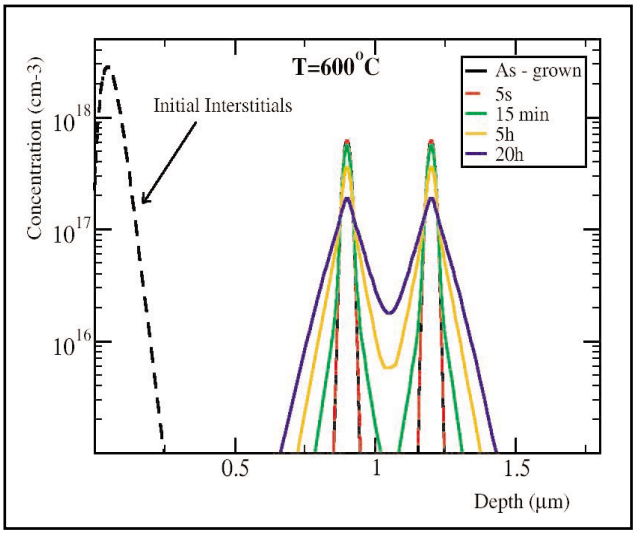

Figure 3. Comparison between experimental and calculated I supersaturation (a), and corresponding calculated B profiles corresponding to ref.[7] (b)

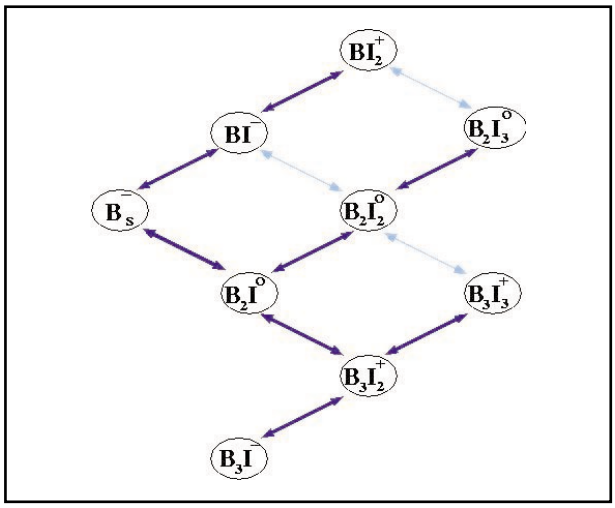

Figure 4. BIC's reaction paths

immobile BIC's are usually invoked to account for the experimental observations, as for example the loss of electrical activity of the dopant. In order to obtain meaningful simulations of the redistribution and activation of implanted B layers, it is thus necessary to model the BIC's formation.

We used here an approach similar to the one used for the IC's, but considering the various possible formation paths : a given cluster can grow or dissolve by the addition or release of a silicon self interstitial or a boron / interstitial pair. In order to reduce the total number of equations to handle, we restricted ourselves to a limited number of BIC's. In absence of any direct experimental data concerning these clusters, we chose the BIC's structures and charge states obtained from a recent ab-initio theoretical calculation [8]. The corresponding formation paths are given on Figure 4. The various kinetics parameters were also computed with the help of the formation and binding energies given in [8].

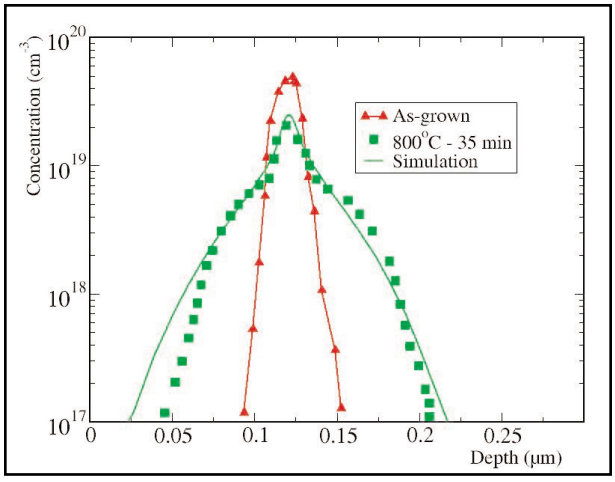

Figure 5.Comparison between experimental and simulated B profiles evidencing the influence of the BIC's. Data are from ref.[9]

The model parameters were eventually tuned by fitting on the experimental profiles of Pelaz et.al., which correspond to the redistribution of a buried B layer, with a peak concentration in the 10^{19} cm^{-3} range, following defect creation by a 2.10^{13} cm^{-2} Si implant, annealed at 800°C for 35 min. Here again we used a simple +1 model to initialize the I concentration. Figure 5 shows the comparison between the calculated and experimental B profiles, and evidences the quality of the simulation.

As a final test of the capability of our fully coupled model to handle all the interactions existing between boron and the free and clustered self-interstitials, we show on Figure 6 the good agreement we obtained for the simulation of the redistribution at 1065°C, 20 sec of a boron profile implanted at 10 keV / 3.10^{15} cm^{-2} (Figure 6).

Conclusion

In this contribution we have shown that, by fully coupling the dopant pair-diffusion model with the kinetics description of the growth and dissolution of the various I-related clusters, it is possible to simulate boron diffusion in a very large range of experimental conditions, from conventional predeposition steps to RTA after low energy implantation.

References

1. N.E.B. Cowern, K.T.F. Jansen and H.F.F. Jos, J. Appl. Phys. 68, 6191 (1990).
2. F. Cristiano, J. Grisiola, B. Colombeau, M. Omri, B. de Mauduit, and A. Claverie, J. Appl. Phys. 87, 842 (2000).
3. D. Mathiot and J.C. Pfister, J. Appl. Phys. 55, 3518 (1984).
4. Orr Arienzo, R.Glang, R.F. Lever and R.K. Lewis, J. Appl. Phys., 63(1),117 (1988).
5. P. Pichler, W. Jungling, S. Selberherr, E. Guerrero, and H. W. Pötzl, IEEE Trans. Computer-Aided Design 4, 384 (1985).
6. C. Ortiz and D. Mathiot, M.R.S. Symp. Proc. 669, J5.6, (2001).
7. N.E.B. Cowern, G.Mannino, P.A. Stolk, F. Roozeboom, H.G.A. Huizing, J.G.M. van Berkum, F. Christiano, A. Claverie, M. Jaraìz, Phys. Rev. Lett. 82, 4460 (1999).
8. J. Lenosky, B.Sadigh, S.K. Theiss, M.-J. Caturla and T.Diaz de la Rubia, Appl. Phys. Lett 77, 1834 (2000).

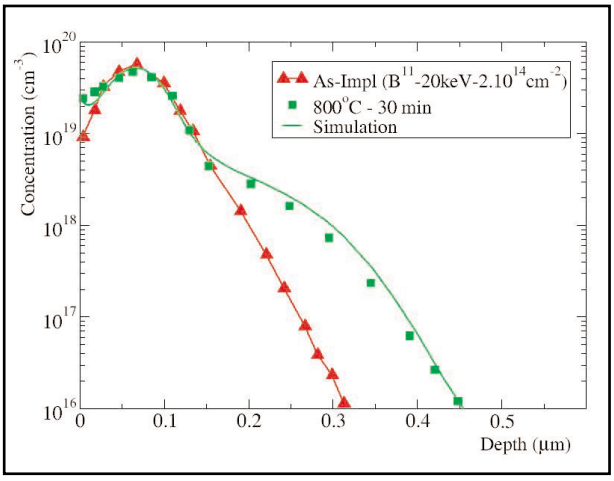

Figure 6. Comparison between experimental and simulated B profiles implanted at 20 keV / 2.1014 cm-2, annealed at 800°C for 30 min.

Breakdown Analysis of a Body-Contacted Submicron High Electron Mobility Transistor

Introduction

Interest continues to grow in the development of high electron mobility transistor (HEMT) technologies for micrometer and millimeter wave power applications. A primary concern of device designers working with such technologies is the breakdown behavior in both the on- and off-states. As is the case for most field-effect transistors, reducing device dimensions results in a larger internal electric field near the drain-end of the device's channel. The presence of such a field within the device can affect many areas of device performance including the breakdown characteristics.

In recent years, several studies [1-3] have examined the on-state and off-state breakdown mechanisms in submicron HEMT technologies. Both experimental and theoretical analysis has shown that a primary mechanism affecting both on-state and off-state breakdown is the accumulation in the channel, buffer, and supply layers of excess holes generated by impact ionization. The accumulated holes act as a positive fixed charge, lowering the energy barrier at the source/channel junction and enhancing the injection of electrons into the channel [2]. This phenomenon is often referred to as the parasitic bipolar effect (PBE).

The additional electrons injected into the channel region due to PBE are accelerated towards the drain further contributing to impact ionization, excess hole generation, and enhanced injection. This positive feedback mechanism ultimately leads to device breakdown and burn-out. In some devices, it has also been shown to cause a kink in the device's output characteristics similar to that seen in silicon-on-insulator (SOI) technologies. The breakdown voltage of the HEMT is reduced as a consequence of the enhanced injection process limiting its power output [2]. Continued improvement of HEMT performance for power applications requires a better understanding of breakdown behavior.

Several approaches have been proposed for improving the breakdown characteristics of power HEMTs including the use of composite channel layers [5], quantum confinement [6], and an additional contact on the device body [4] to suppress impact ionization. This article follows the work of Sleiman et al [4] and examines the use of a body contact to improve the breakdown performance of a 250 nm psuedomorphic high electron mobility transistor. Further, this article will illustrate how ***Blaze***, Silvaco's 2D device simulator for advanced materials, can be used to analyze the internal mechanisms of a common device technology. The analysis methods shown are applicable to a wide range of common device technologies.

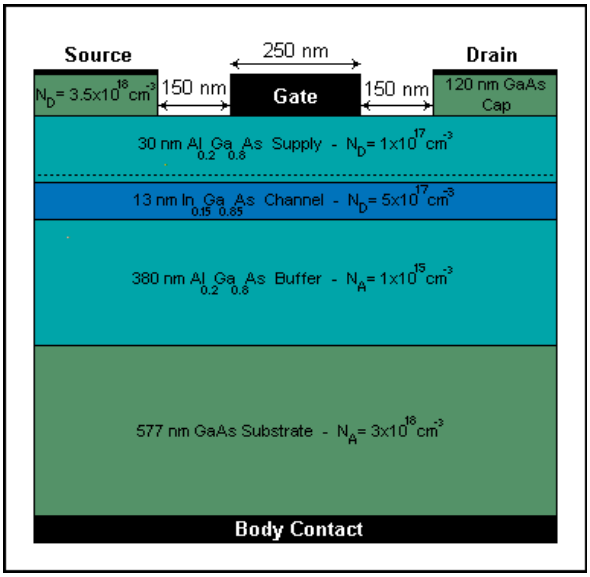

Figure 1. Schematic cross section of the simulated submicron psuedomorphic body-contacted HEMT

Simulated Device

A schematic diagram of the simulated body-contacted HEMT structure is shown in Figure 1. The primary dimensions and doping values used for this study are shown. The dashed line extending across the bottom of the AlGaAs Supply layer represents a region of delta-doping. The delta-doping lies 2 nm from the Supply/Channel interface and has a peak density of 1x10^{12} cm^{-2}. Highly n-doped regions (peak concentration = 5x10^{21} cm^{-3}) also exist directly beneath the source and drain electrodes, but are not shown. These regions extend to the top of the InGaAs Channel layer.

For comparison, a second HEMT structure without a body contact was also simulated. This structure, referred to as the base HEMT, is identical to the body-contacted structure shown in Figure 1 with the following exceptions: 1) the body contact was removed, and 2) the GaAs substrate is lowly doped (NA = 1x10^{15} cm^{-3}). The breakdown characteristics of both devices were simulated using the standard drift-diffusion approach. Appropriate models for Shockley-Read-Hall, Auger, and direct recombination were included. Carrier generation resulting from impact ionization was accounted for using the Selberherr impact ionization model. A full description of each device model is available within the ***ATLAS*** *User's Manual* [7].

It should be noted that the simulation approach used in this study represents a simplified model set. As applied, the drift-diffusion solution includes the

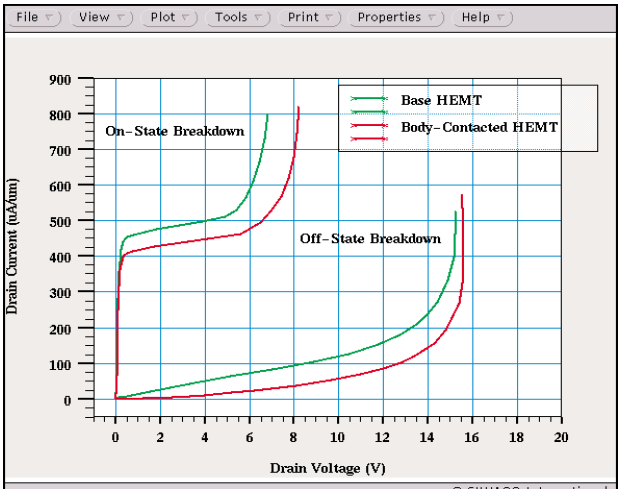

Figure 2. Simulated HEMT breakdown characteristics for both the Base and Body-Contacted HEMT structures. On-state simulations conducted at VG = -0.4 V; Off-state simulations conducted at VG = 0.8 V.

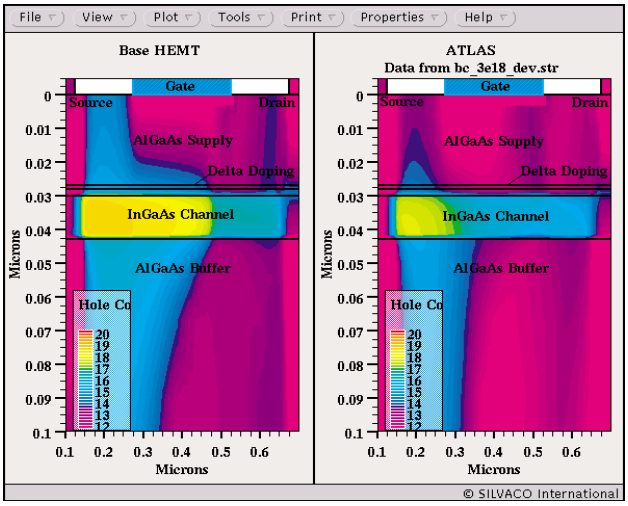

Figure 3. 2D device cross section taken from base and body-contacted HEMT structures with overlain contours of hole concentration (cm^{-3}).

following assumptions: 1) carrier velocity and mobility are functions of the local electric field, and 2) carrier temperature is equal to the lattice temperature which was 300 K for this study. As such, non-local transport effects such as velocity-overshoot were not accounted for.

A more advanced approach including non-local affects and carrier energy variations would be more accurate, however as shown by [8], a drift-diffusion approach neglecting non-local transport effects is adequate for the qualitative analysis of HEMT breakdown resulting from impact ionization. For an in-depth discussion of the advanced transport models available in ***Blaze*** please refer to the article "2D Simulation of Psuedomorphic Heterojunction Devices Using the Fully-Coupled Carrier Energy Balance Model" as published in the April 1995 *Simulation Standard* newsletter. A copy of this article is available online at **www.silvaco.com/simstd/simstd.html**.

It has been proposed by some that off-state breakdown is dominated by a combination of thermionic emission and tunneling [9]. Investigation of this idea was determined to be beyond the scope of this work and will be left to future discussion.

Results and Discussion

Figure 2 presents the breakdown characteristics of both the base and body-contacted HEMT structures. The on-state and off-state breakdown curves were extracted at VG = 0.8V and VG = -0.4V, respectively. The body-contacted HEMT shows an improvement in breakdown performance of nearly 2V. This figure agrees well with the results published in [4]. The on-state breakdown simulation does highlight one potential limitation of the body-contact approach. The saturation current of the body-contacted device is substantial lower than that of the conventional HEMT. At VD = 5V, the drain current in the body-contacted device is 60 uA/um less than that of the base HEMT. This is a direct result of the holes being removed from the active device through the body contact.

Figure 3 shows the contours of hole concentration across the supply, channel, and buffer regions of the base and body-contacted devices under on-state breakdown conditions. As can be seen, the concentration of holes near the source-end of the channel in the back-contacted device is substantially lower than in the base HEMT. This is more clearly seen in Figure 4 which shows the hole concentration across the lateral width of the channel layer 5nm beneath the supply/channel interface. The hole concentration at the source-end of the channel has been reduced by an order of magnitude. The difference at the middle of the channel is even more dramatic.

The off-state breakdown characteristics of the body-contacted device do not show as significant an improvement as the on-state characteristics. Again for

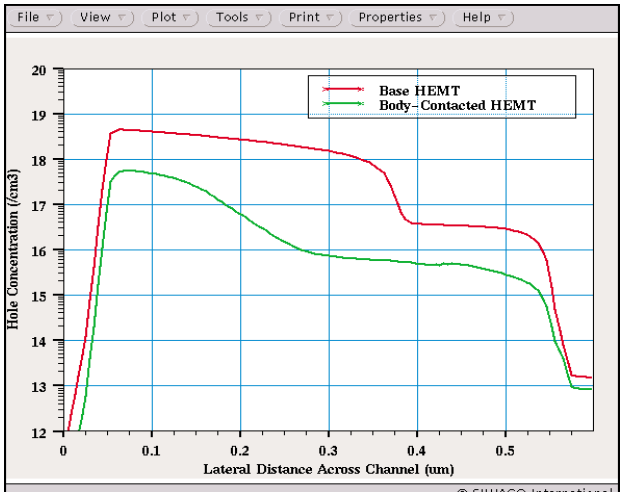

Figure 4. Hole concentration across device channel at on-state breakdown

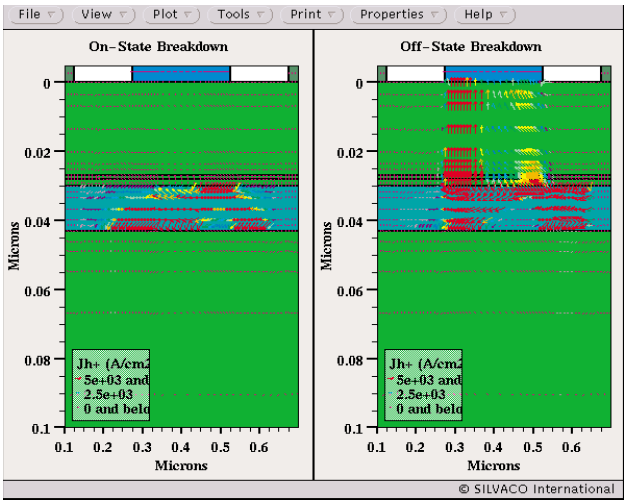

Figure 5. Hole current density vectors for the body-contacted HEMT under a) on-state breakdown (VG = 0.8V, VD = 7V) b) off-state breakdown (VG = -0.4V, VD = 15V).

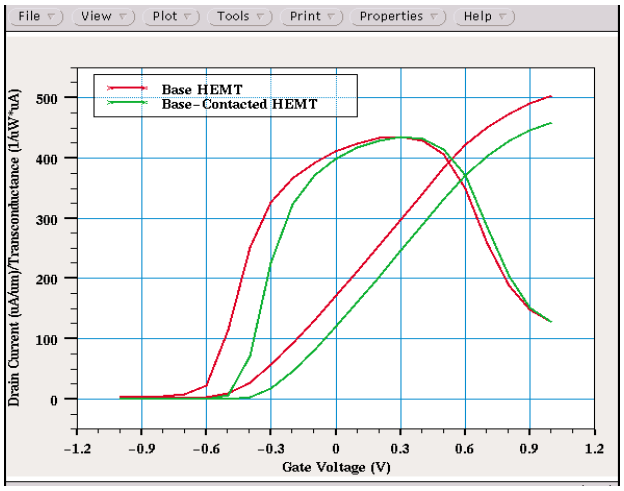

Figure 6. Subthreshold characteristics for base and body-Contacted HEMT Structures. Characteristics extracted at VD = 2V.

the body-contacted device, the drain current prior to breakdown has been reduced in comparison to that of the conventional device, however the breakdown voltage itself is only improved by about 1V. This indicates that off-state breakdown is not as dependent on hole accumulation as on-state breakdown. It may also be possible that under off-state conditions a portion of the accumulated holes are removed through the gate electrode thereby reducing the impact of the back contact.

Figure 5 shows the hole current density vectors across the supply, channel, and buffer regions of the body-contacted device under both on- and off-state breakdown. As can be seen, the is a considerable amount of hole current flowing through the gate electrode under the off-state breakdown conditions. This supports the idea that the presence of the body contact has less of an effect on off-state breakdown behavior. Figure 6 shows the subthreshold characteristics of both the base and body-contacted HEMT structures. Extracted at VD = 2V, the subthreshold characteristics do not indicate any other significant design trade-offs resulting from the presence of the body contact. Both the drain current and conductance values are shifted to a slightly higher gate voltage.

Summary

An important component of HEMT design for power applications is the breakdown behavior of the device in both the on- and off-states. Similar to other field effect devices, the breakdown behavior of HEMTs is adversely affected by the large electric fields present within submicron structures. To further improve HEMT performance, a better understanding of the on-state and off-state breakdown mechanisms and methods for controlling these mechanisms is needed. Device simulation provides an excellent tool for analyzing these mechanisms and developing new device structures for minimizing their effects.

This article examined the effect of hole accumulation and the parasitic bipolar effect on the on-state and off-state breakdown behavior of a 250 nm psuedomorphic body-contacted HEMT structure through the use of a standard drift-diffusion approach. To obtain a better understanding of these mechanisms, the breakdown behavior of the body-contacted device was compared to that of a conventional HEMT structure of similar build. The presence of the body contact was shown to increase the breakdown voltage of the device under both on- and off-state conditions at the expense of a lower drain saturation current.

References

[1] M. Somerville et al., "A New Gate Current Extraction Technique for Measurement of On-State Breakdown Voltage in HEMT's," IEEE Electron Device Letters, vol. 19, pp.405-407, November 1998.

[2] A. Di Carlo et al., "Monte Carlo Study of the Dynamic Breakdown Effects in HEMT's," IEEE Electron Device Letters, vol. 21, pp. 149-151, April 2000.

[3] R. Shigekawa et al., "Electroluminescence of InAlAs/InGaAs HEMT's Lattice-Matched to InP Substrates," IEEE Electron Device Letters, vol. 16, pp. 515-517, November 1995.

[4] A. Sleiman et al., "Breakdown Quenching in High Electron Mobility Transistor by Using Body Contact," IEEE Transactions on Electron Devices, vol. 48, pp. 2188-2191, October 2001.

[5] T. Enoki et al., "Design and Characteristics of InGaAs/InP Composite-Channel HFET's," IEEE Transactions on Electron Devices, vol. 42, pp. 1413-1418, August 1995

[6] C. R. Bolognesi et al., "Impact Ionization Suppression by Quantum Confinement: Effects on the DC and Microwave Performance of Narrow-Gap Channel InAs/AlSb HFET's," IEEE Transactions on Electron Devices, vol. 46, pp. 826-832, May 1999.

[7] *ATLAS User's Manual,* Silvaco International, November 1998.

[8] K. Eisenbeiser et al., "Theoretical Analysis of the Breakdown Voltage in Psuedomorphic HFET's," IEEE Transactions on Electron Devices, vol. 43, pp. 1778-1787, November 1996.

[9] M. Somerville et al., "Off-State Breakdown in Power pHEMT's: The Impact of the Source," IEEE Transactions on Electron Devices, vol. 45, pp. 1883-1889, September 1998.

QUEST: Frequency-Dependent RLCG Extractor

Part 2 - Comparison with Experiments

Introduction

This article presents a standard case of transmission line: the microstrip structure. First, the structure is described and then the results extracted from ***QUEST*** are compared with measurements. We thank STMicroelectronics (Crolles-R&D) for experimental data support.

1. Microstrip Structure

This structure represents a line screened from the silicon substrate by a metallic plate. Figure 1 shows the microstrip structure used for the simulation in QUEST.

The plate and the line are 100 µm and 4 µm wide respectively. Though the substrate is screened, it must be defined for simulation purpose. Figure 2 shows the definition of the parameterized materials in QUEST in the Process menu, whereas Figure 3 shows the mesh parameters in the Field Solver menu.

The number of Z-slices in the 'pass1' layer is adjusted to take into account the skin effect in the metal line.

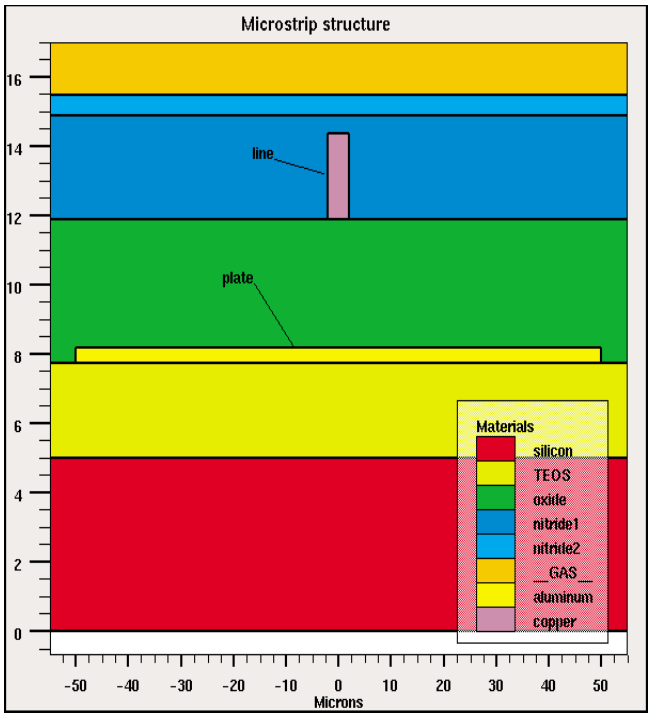

Figure 1. The microstrip structure.

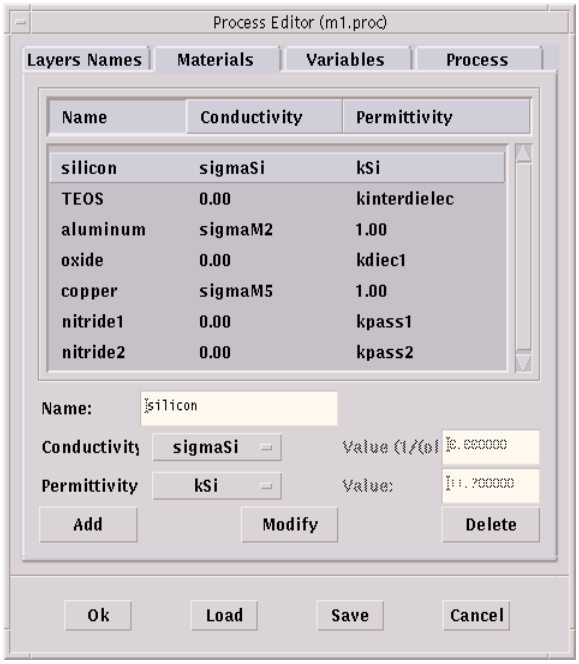

Figure 2. Definition of the materials

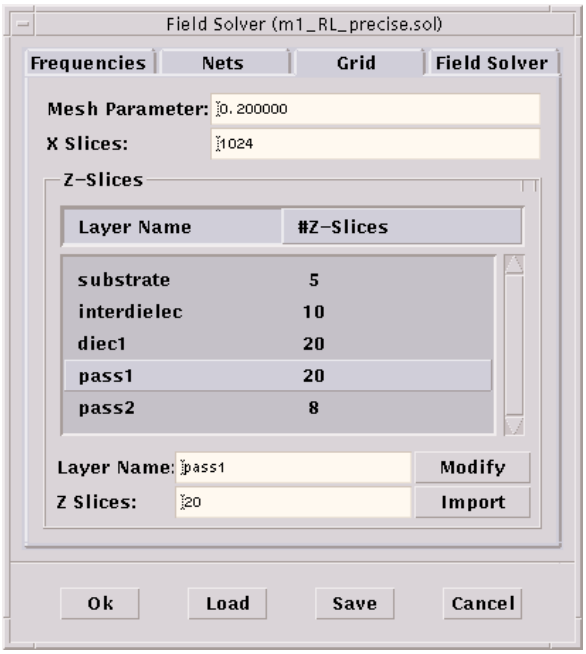

Figure 3. Mesh generation.

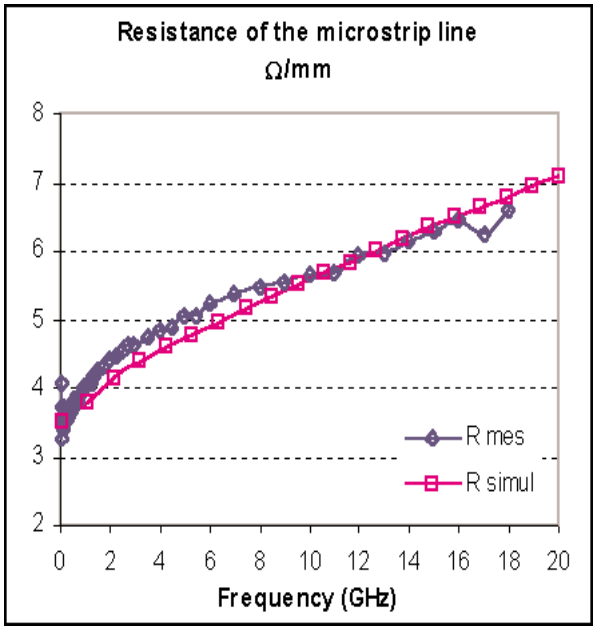

Figure 4. Ccomparison of measured and simulated resistance.

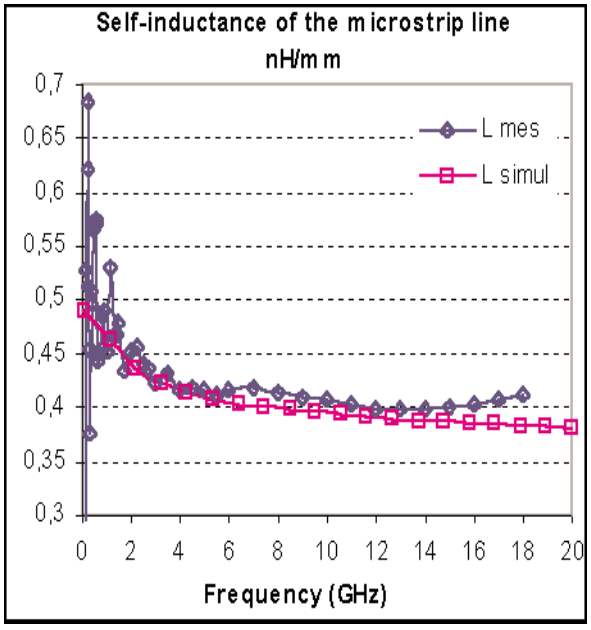

Figure 5. Ccomparison of measured and simulated self-inductance.

2. Results

In order to compare simulated results with measurements, attention should be paid on the current return path. In QUEST, the reference is the substrate by default whereas the experiments have been performed in such a way that the reference is the plate. The default in ***QUEST*** has to be changed by selecting a flag setting the plate as the reference for the current return path.

Figures 4, 5 and 6 reports respectively the line resistance R, the self-inductance L and the capacitance C per unit length as measured and calculated by ***QUEST***.

Concerning the R and L, the simulated data are closed to the experimental ones. For the capacitance, the average difference is greater than 5%. This difference can be explained by the difference in topology between the simulated structure and the experimental one.

Conclusion

Simulated results have been compared to experimental data on a microstrip structure. A good agreement is obtained between simulated and experimental data. This comparison shows that ***QUEST*** is a reliable tool to extract the lumped elements of a microstrip line. The reader will find other comparison in [1].

Reference

[1] Performance Characterization of Advanced Interconnects on High Speed VLSI Circuits, C.Bermond, ESSDERC 2000.

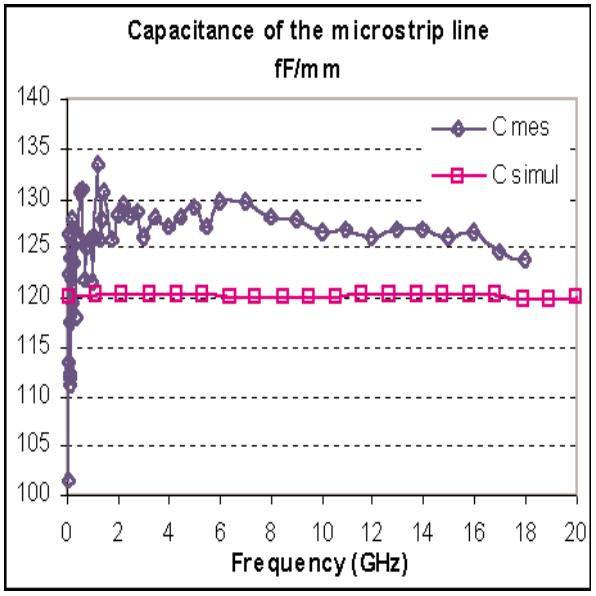

Figure 6. Comparison of measured and simulated capacitance.

Calendar of Events

May

1	
2	
3	
4	
5	
6	
7	
8	
9	
10	
11	
12	
13	
14	
15	
16	
17	
18	
19	CLEO - Long Beach, CA
20	CLEO - Long Beach, CA
21	CLEO - Long Beach, CA
22	CLEO - Long Beach, CA
23	CLEO - Long Beach, CA
24	CLEO - Long Beach, CA
25	
26	ISCAS - Scottsdale, AZ
27	ISCAS - Scottsdale, AZ
28	ISCAS - Scottsdale, AZ
29	ISCAS - Scottsdale, AZ
30	
31	

June

1	
2	HITEC - Albuquerque, NM
3	HITEC - Albuquerque, NM ISPSD - Santa Fe, NM IITC - San Francisco, CA
4	HITEC - Albuquerque, NM ISPSD - Santa Fe, NM IITC - San Francisco, CA
5	HITEC - Albuquerque, NM ISPSD - Santa Fe, NM IITC - San Francisco, CA
6	ISPSD - Santa Fe, NM
7	ISPSD - Santa Fe, NM
8	
9	
10	DAC - New Orleans, LA IWSM - Kyoto, Japan
11	DAC - New Orleans, LA IWSM - Kyoto, Japan
12	DAC - New Orleans, LA IWSM - Kyoto, Japan
13	DAC - New Orleans, LA IWSM - Kyoto, Japan
14	DAC - New Orleans, LA IWSM - Kyoto, Japan
15	
16	
17	
18	
19	
20	
21	
22	
23	
24	ADRC - UC Santa Barbara
25	ADRC - UC Santa Barbara
26	ADRC - UC Santa Barbara
27	
28	
29	
30	

Bulletin Board

Meeting Customers Needs Through Linux Porting

Silvaco International understands the need for modern designers to comply with a budget while not sacrificing performance. In recent years the Linux platform has been emerging as a tool to meet that need. Silvaco's Utmost (Data Acquisition & Parameter Extraction) is now available on the Linux platform. Silvaco's line of design, layout and verification tools (***CELEBRITY***) are also slated for a spring release on the Linux platform. We are pleased to further meet this need by porting every one of our tools to Linux by June 2002.

Silvaco To Attend NSREC

Silvaco International intends to further develop and nurture it's already diverse military, space and Rad Hard foundation by attending this years NSREC (Nuclear & Space Radiation Effects Conference.) Held in Phoenix, Arizona at the Pointe South Mountain Resort on July 15-19, 2002. This annual meeting of engineers and scientists presents the latest techniques for enhancing the performance of microelectronic devices and circuits that are used in radiation environments. Silvaco will be showcasing it's diverse TCAD tool set, come see us at booth #2.

See You in New Orleans

Silvaco International will be showcasing its extensive suite of TCAD tools this year at DAC in New Orleans, Louisiana. Silvaco has become the industry standard for TCAD Driven CAD tools throughout the world by providing hundreds of leading companies with tools that increase productivity, accuracy, and ease of use. Come see Silvaco at booth #2917 to meet with our seasoned engineers and software developers, and they will demonstrate how Silvaco provides "the right tools for the job".

If you would like more information or to register for one of our our workshops, please check our web site at ***http://www.silvaco.com***

Hints, Tips and Solutions

William French, Applications and Support Manager

Q. Can *ATLAS* simulate a Schottky contact ?

ATLAS allows the user to define a contact with a number of different boundary conditions; ohmic, Schottky, current controlled, floating or reflecting.

The Schottky contact boundary condition realizes that at the metal semiconductor interface a barrier exists due to the presence of interface states. A special surface potential is applied at this contact that is calculated according to

$$\Psi_s = \text{AFFINITY} + \frac{E_G}{2q} + \frac{kT}{2q} \ln \frac{N_c}{N_v} - \text{WORKFUN} + \text{Vapplied}$$

where AFFINITY is the electron affinity of silicon and WORKFUN is the workfunction of the metal contact. For example, if the Schottky contact was aluminum with a workfunction difference to the silicon of 4.2 eV and the barrier height was 0.7 eV, then the user would define the Schottky contact with the statement

CONTACT NAME=GATE WORKFUN=4.9

The WORKFUN parameter is the aluminum workfunction plus the barrier height. This is all that is needed by the simulation to simulate a Schottky contact.

As an example of this type of simulation a Schottky diode and a regular p+/n+ diode have been simulated within ***ATLAS***. The Schottky diode has been simulated with the first technique described above and consists of an aluminum contact on 1e14 cm-3 n- type silicon where a barrier height of 0.7 eV has been assumed at the contact. The mesh was carefully created to ensure that under the Schottky contact the mesh density was sufficient to resolve the depletion region. The chosen set of models were

MODELS FERMI SRH CVT AUGER

Fermi-Dirac statistics were chosen to ensure proper simulation of high carrier concentration statistics, SRH to model thermal recombination and generation, CVT was the chosen mobility model and AUGER to model carrier-carrier recombination.

Figure 1 shows the two structures that were simulated and Figure 2 shows the I-V characteristics of the Schottky and regular diodes on a log scale. The simulation shows several important effects

- the Schottky diode turns on at a lower voltage than the p+/n+ diode

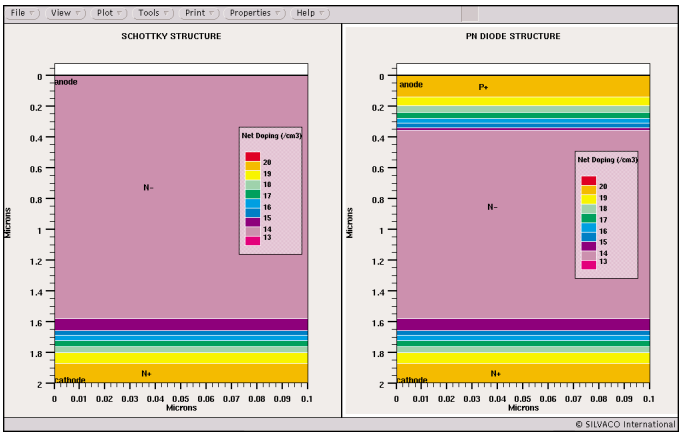

Figure 1. The structures simulated were a Schottky diode and a pn diode. In the Schottky case the anode contact was the Schottky contact.

- the Schottky diode exhibits forward current saturation at much lower current levels than the diode
- the Schottky diode has much higher leakage current than the p+/n+ diode

These are the well known features of a Schottky diode which are made use of in many modern technologies.

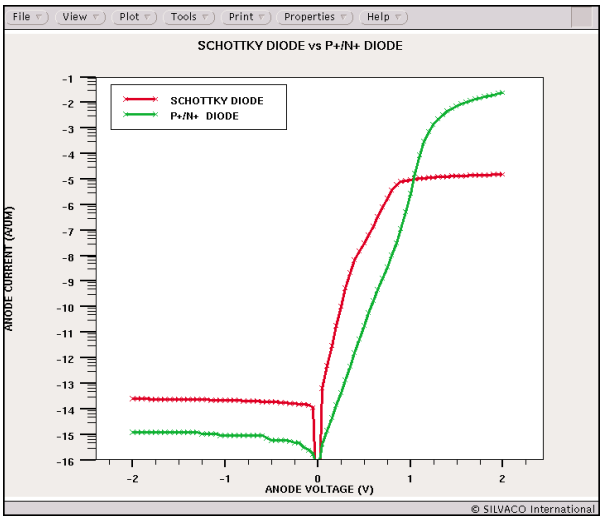

Figure 2. Simulated IV characteristics of the Schottky and pn diodes.

Call for Questions

If you have hints, tips, solutions or questions to contribute, please contact our Applications and Support Department

Phone: (408) 567-1000 Fax: (408) 496-6080

e-mail: *support@silvaco.com*

Hints, Tips and Solutions Archive

Check our our Web Page to see more details of this example plus an archive of previous Hints, Tips, and Solutions

www.silvaco.com

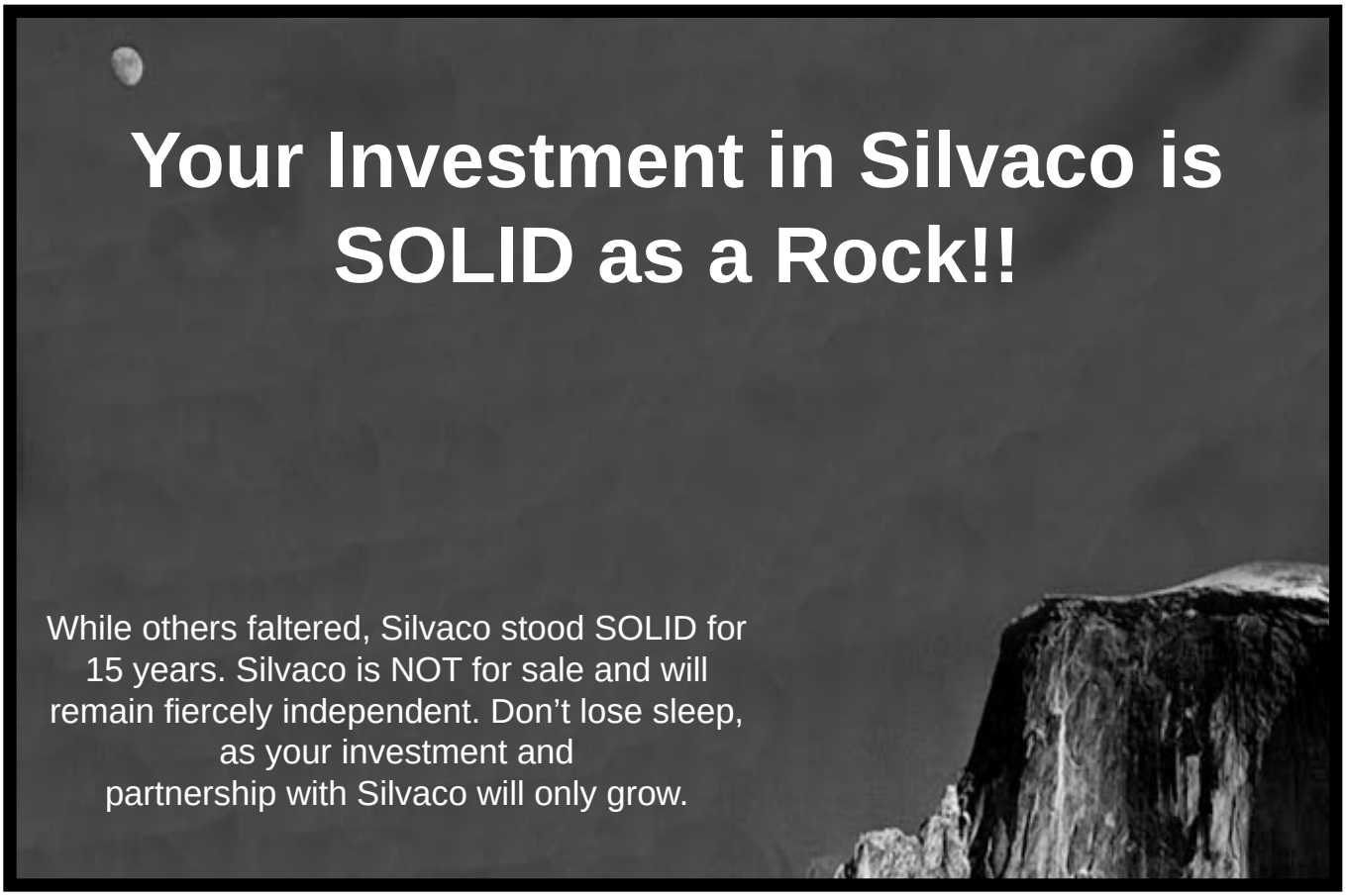

SILVACO INTERNATIONAL

USA Headquarters

Silvaco International
4701 Patrick Henry Drive
Building 2
Santa Clara, CA 95054
USA

Phone: 408-567-1000
Fax: 408-496-6080

sales@silvaco.com
www.silvaco.com

Contacts:

Silvaco Japan
jpsales@silvaco.com

Silvaco Korea
krsales@silvaco.com

Silvaco Taiwan
twsales@silvaco.com

Silvaco Singapore
sgsales@silvaco.com

Silvaco UK
uksales@silvaco.com

Silvaco France
frsales@silvaco.com

Silvaco Germany
desales@silvaco.com

Products Licensed through Silvaco or e*ECAD

e*ECAD
Vendor Partner